







HO-Cap: A Capture System and Dataset for 3D Reconstruction and Pose Tracking of Hand-Object Interaction

Jikai Wang¹, Qifan Zhang¹,
Yu-Wei Chao², Bowen Wen², Xiaohu Guo¹, and Yu Xiang¹

¹ University of Texas at Dallas, Richardson TX 75080, USA
{jikai.wang, qifan.zhang, xguo, yu.xiang}@utdallas.edu
² NVIDIA {bowenw, ychao}@nvidia.com

Abstract. We introduce a data capture system and a new dataset named HO-Cap that can be used to study 3D reconstruction and pose tracking of hands and objects in videos. The capture system uses multiple RGB-D cameras and a HoloLens headset for data collection, avoiding the use of expensive 3D scanners or mocap systems. We propose a semi-automatic method to obtain annotations of shape and pose of hands and objects in the collected videos, which significantly reduces the required annotation time compared to manual labeling. With this system, we captured a video dataset of humans using objects to perform different tasks, as well as simple pick-and-place and handover of an object from one hand to the other, which can be used as human demonstrations for embodied AI and robot manipulation research. Our data capture setup and annotation framework can be used by the community to reconstruct 3D shapes of objects and human hands and track their poses in videos. ³

Keywords: Dataset Construction · Hand-Object Interaction · Hand Pose Estimation · 3D Object Reconstruction · Object Pose Estimation

1 Introduction

Understanding hand-object interaction from images or videos has been an active research topic in computer vision due to its wide applications in human-computer interaction, VR/AR and robot learning from human demonstration. Specific problems such as hand detection [31, 49], hand pose estimation [15, 16], hand shape reconstruction [33, 36, 41], hand-object detection [10, 37], object pose estimation [6, 25, 44, 45], and object shape reconstruction [8, 43, 48] are actively studied in the community. Meanwhile, to facilitate research and benchmarking of these problems, several datasets related to hands and objects have been introduced in recent years [7, 13, 20, 23, 28, 47]. Most datasets consist of videos of

³ Data, code and videos for the project are available at
<https://irvlutd.github.io/HOCap>

users manipulating objects in front of some cameras, and then ground truth annotations such as hand poses and object poses are obtained in different ways.

An easy way to obtain pose annotations is to use motion capture (mocap) systems [4, 13]. However, mocap systems are not only expensive, but also introduce artificial markers on hands and objects during data capture. On the other hand, several datasets are constructed by manual labeling such as DexYCB [7], OakInk [47] and HOI4D [28]. With a large number of video frames, human annotation is very time-consuming. Recently, a few systems have been proposed to automatically or semi-automatically compute pose annotations for hands and objects [18, 23]. However, these systems are not scalable to various objects or hand-object interactions. For example, HO-3D [18] used objects with known 3D models. It cannot handle unseen objects. H2O [23] needs to train an object tracker for each captured object, which makes it not scalable to the number of objects.

In this work, we introduce a new capture system and a new dataset for hand-object interaction. The capture system uses eight calibrated RGB-D cameras and a HoloLens headset [1] for both third-person and ego-centric views. A semi-automatic annotation method is introduced which can obtain accurate annotations of 3D shapes and poses of hands and objects in videos. Our method does not rely on any marker for motion capture or on expensive 3D scanners to reconstruct 3D models of objects. Additionally, no domain-specific training is required. These properties make our capture system scalable and easily deployable for hand-object interaction, compared to previous systems [18, 23].

Specifically, we leverage recent advances brought by large-scale pre-trained vision models, such as MediaPipe [30] for hand detection and pose estimation, BundleSDF [42, 43] for 3D object reconstruction and pose estimation, and SAM [22] and XMem [9] for object segmentation and tracking. To handle noises and errors from the prediction results of these models, we leverage multi-view consistency with eight RGB-D cameras. Furthermore, a Signed Distance Field (SDF)-based optimization method is proposed to refine the hand pose and the object pose in the 3D space. Consequently, our annotation pipeline can automatically process captured RGB-D videos and generate 3D shape and pose of hands and objects. The only human annotation required is to manually prompt two points for each object in the first frame to generate an initial segmentation mask of the object using SAM [22], and label the name of the object to associate it to an object in our database.

Using our data capture system and annotation method, we constructed a new dataset named HO-Cap, for hand-object interaction research. The dataset contains human demonstration videos of unimanual or bimanual interaction with objects. We consider three types of interaction: affordance-driven object uses, object pick-and-place, and handing an object from one hand to the other. The dataset provides 70 videos of 699K RGB-D frames, in which 9 subjects used 64 objects to perform various tasks. Ground truth annotations of 3D shape and pose of human hands and objects are generated for every frame in the dataset



Fig. 1: Examples of RGB frames and the 3D shape and pose annotations of hands and objects in our dataset.

using our annotation pipeline. Fig. 1 illustrates some example images and their annotations in our dataset.

Our dataset can be useful for studying several hand-object recognition problems. In this paper, we provide baseline experimental results for CAD-based object detection, open-vocabulary object detection, hand pose estimation, and unseen object pose estimation. Our goal is to use the dataset as a test bed for testing zero-shot capabilities of different models for hand-object recognition. These models can be trained on external data other than those from our dataset. In this way, our dataset can be helpful for testing large models trained for hands or objects. Another potential usage of our dataset is to utilize the trajectories of hands and objects as human demonstrations for research on embodied AI and robot manipulation.

In summary, our contributions of this work are as follows.

- We introduce a capture system and a scalable semi-automatic annotation method to obtain 3D shape and pose of hands and objects from multi-view RGB-D videos.
- We introduce a new dataset for hand-object interaction that focuses on humans using objects to perform tasks. It covers diverse grasping and multi-object rearrangement tasks, which are novel and valuable to the imitation learning community.
- We provide a benchmark with several baseline results for the task of zero-shot object detection, hand pose estimation, and object pose estimation.

2 Related Work

In recent years, a number of hand-object interaction datasets have been introduced. Representative datasets are summarized in Table 1 compared to ours. In the following, we discuss in more detail the data capture and annotation process of these datasets.

Table 1: Comparison of our HO-Cap with recent hand-object interaction datasets.

dataset	year	modality	#seq.	#frames	#subj.	#obj.	#views	real image	marker-less	bi-manual	object reconst.	task	label
FPHA [14]	2018	RGB-D	1,175	105K	6	4	ego	✓	×	×	×	multi-task	mocap
Obman [19]	2019	RGB-D	–	154K	20	3K	1	×	✓	×	×	grasping	synthetic
HO-3D [18]	2020	RGB-D	27	78K	10	10	1-5	✓	✓	×	×	grasping & manipulation	automatic
ContactPose [4]	2020	RGB-D	2,303	2,991K	50	25	3	✓	×	✓	×	grasping & manipulation	mocap & thermal
GRAB [40]	2020	mesh	1,335	1,624K	10	51	–	×	×	✓	×	grasping	mocap
DexYCB [7]	2021	RGB-D	1,000	582K	10	20	8	✓	✓	×	×	grasping & handover	manual
H2O [23]	2021	RGB-D	–	571K	4	8	4+ego	✓	✓	✓	✓	multi-task	semi-auto
OakInk [47]	2022	RGB-D	792	230K	12	100	4	✓	×	×	✓	multi-task	manual
HOI4D [28]	2022	RGB-D	4,000	2,400K	4	800	ego	✓	✓	×	✓	multi-task	manual
AffordPose [20]	2023	mesh	–	–	–	641	–	×	–	×	×	multi-task	synthetic
SHOWMe [39]	2023	RGB-D	96	87K	15	42	1	✓	✓	×	✓	grasping	semi-auto
ARCTIC [13]	2023	RGB	399	2,100K	10	11	8+ego	✓	×	✓	✓	bimanual manipulation	mocap
Ours	2024	RGB-D	70	699K	9	64	8+ego	✓	✓	✓	✓	multi-task	semi-auto

Mocap vs. Natural capture. A straightforward way to obtain hand pose and object pose is to use mocap systems. By attaching reflective markers to the hands and objects, a mocap system can track these markers to obtain the hand pose and the object pose. For example, FPFA [14], ContactPose [4] and ARCTIC [13] used mocap systems to obtain ground truth pose annotations. Although mocap systems simplify the data annotation process, they are expensive and introduce artificial patterns into the scene. Additionally, image cameras must be calibrated with mocap cameras to provide image data. Therefore, in this work, we set up a multi-camera system for data capture. We do not need to have markers on hands or objects in our dataset.

Manual labeling vs. Automatic labeling. Recent large-scale hand-object datasets such as DexYCB [7], OakInk [47] and HOI4D [28] are manually labeled. Despite the fact that the quality of the annotation can be guaranteed, the laborious process makes them untenable to scale. On the other hand, several datasets are constructed with automatic labeling such as HO-3D [18] or semi-automatic labeling such as H2O [23] and SHOWMe [39]. Fully automated algorithms for annotation may suffer from annotation errors. Existing semi-automatic annotation methods incorporate manual correction of errors [23] or manually initialize a tracking process to annotate videos [39]. Recently, HANDAL [17] proposed a semi-automatic annotation pipeline to obtain ground-truth 6D object poses. However, it only provides a small number of dynamic human-object interaction sequences and does not provide hand annotations. In our work, we introduce a new semi-automatic pipeline for annotating 3D shape and pose of both hands and objects in videos. The only human label required is the selection of two points on the object in the first frame, i.e., point prompts for segmenting objects with SAM [22]. The method can then automatically process the remaining video frames to obtain annotations. As highlighted in Table 1, our dataset contains markerless unimanual and bimanual videos. Our annotation method can reconstruct 3D shapes of novel objects. The most similar work to ours is H2O [23]. Unlike H2O, we do not need to train object pose trackers for the captured objects with domain-specific training data. By utilizing pre-trained

large-scale vision models with our multi-camera setup, our annotation method is more scalable to different kinds of hand-object interaction.

3 Data Capture Setup

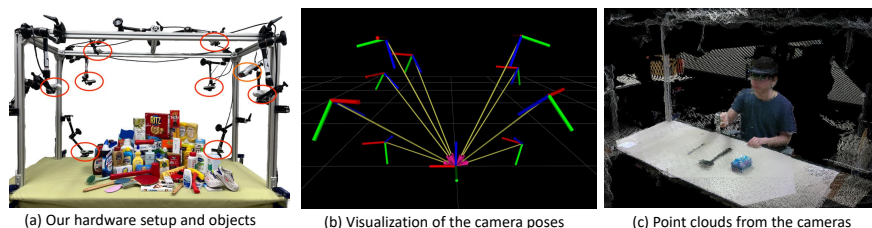


Fig. 2: Illustration of our data capture setup.

Our hardware setup is illustrated in Fig. 2(a). We set up 8 Intel RealSense D455 cameras and 1 Microsoft Azure Kinect [2] above a table. All these cameras can capture RGB-D videos. The Azure Kinect camera is mainly used for collecting images for 3D object reconstruction, since it has a higher resolution than the RealSense cameras. The eight RealSense cameras are configured to have good coverage of the workspace. After installing the cameras, we have already calibrated the intrinsics and extrinsics of these cameras using the Vicalib calibration tool [3]. Fig. 2(b) visualizes the camera poses in 3D using RGB-colored axes. The axes in the center indicate the tabletop. After calibration of these cameras, we can fuse the point clouds from these cameras to a common 3D coordinate frame. Fig. 2(c) shows an example of a point cloud from all cameras.

In addition to RGB-D videos and point clouds from these static cameras, we ask users to wear a Microsoft HoloLens AR headset [1] during data collection (see Fig. 2(c)). In this way, we can also collect ego-centric view RGB-D videos using the cameras on the HoloLens glasses. We provide synchronized first-person view and third-person view RGB-D videos in our dataset. We also track the 6D poses of the HoloLens glasses in the workspace. Therefore, we can fuse the point clouds from the HoloLens glasses with the point clouds from the RealSense cameras.

4 Annotation Method

After setting up the capture system, our goal is to provide 3D shape and pose of hands and objects in the collected videos. A critical requirement is the ability to handle arbitrary objects whose 3D models were not available before the capture. We propose a semi-automatic annotation method based on our multi-view camera setup, without using expensive 3D scanners or mocap systems.

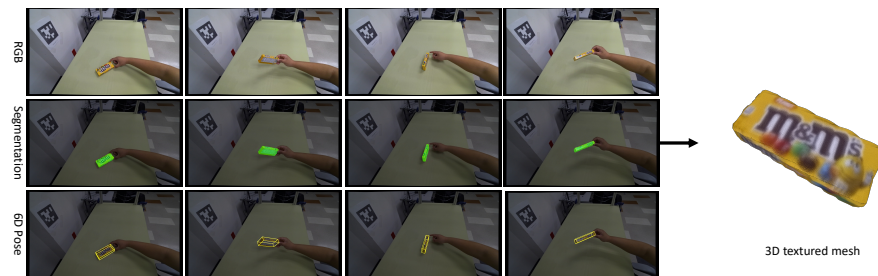


Fig. 3: Illustration of our pipeline for 3D object reconstruction.

4.1 3D Object Reconstruction

Our annotation process starts with acquiring 3D models for the objects to be manipulated. We assume that the objects are rigid. Instead of using objects with known 3D meshes, such as from the YCB Object Set [5] or using 3D scanners to obtain 3D meshes [39], we use a recent neural object reconstruction method, BundleSDF [43], to reconstruct a textured 3D mesh for each object. BundleSDF uses a sequence of RGB-D images in conjunction with the object’s segmentation masks to precisely track its 6D pose and reconstruct its textured mesh. As a result, we can simply use an RGB-D camera for object reconstruction and obtain 3D meshes for a variety of objects. The 3D object reconstruction process is illustrated in Fig. 3.

To prepare the input data, we manually move and rotate an object in front of the Azure Kinect camera, ensuring exhaustive coverage of the surfaces, which is critical for the fidelity of the object reconstruction. To accurately delineate the object masks throughout the image sequence, we prompt the Segmentation Anything Model (SAM) [22] with two manually selected points on the first frame to generate the initial segmentation mask of the object. This manual prompting is designed to ensure high accuracy in the initial mask in order to bootstrap the subsequent automated mask tracking. When the initial mask is established, we use XMem [9], an object-agnostic video segmentation method, to track the object mask in the remaining frames of the video sequence.



Fig. 4: Reconstructed textured meshes of the 64 objects in HO-Cap

Given the object masks, BundleSDF uses feature matching based on LoFTR [38] to perform a coarse pose initialization followed by an online pose graph optimization to estimate the 6D poses of objects in the video frames. Meanwhile, a neural object field is trained in parallel for modeling the object-centric ge-

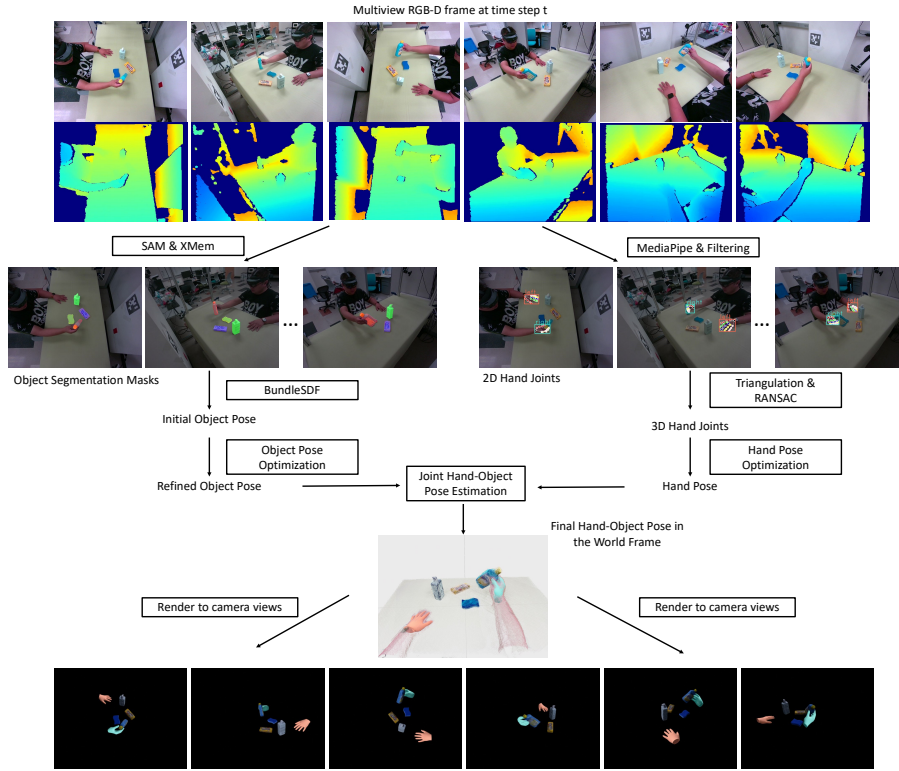


Fig. 5: Illustration of our pipeline for obtaining poses of hands and objects from multi-view RGB-D videos.

ometry and appearance information, while it simultaneously refines the poses of the keyframes to reduce tracking drift. Finally, a textured 3D mesh can be extracted from the neural object field via marching cubes [29] combined with color projection. In total, we reconstructed 64 objects in our dataset as shown in Fig. 4. These objects can be easily purchased online.

4.2 Object Pose Estimation

After obtaining the 3D models of objects, we use them to represent and estimate the object poses in the videos where the subjects are performing the actual tasks with these objects. Our pipeline for pose estimation of hands and objects is illustrated in Fig. 5.

Object Pose Initialization In our framework, the pose of each object is a homogeneous transformation $\mathbf{T} = (\mathbf{R}, \mathbf{t}) \in \mathbb{SE}(3)$, where \mathbf{R} and \mathbf{t} are the 3D rotation and the 3D translation of the object mesh frame with respect to the world frame, respectively. The world frame is defined near the center of the table, as shown in Fig. 2(b). Since all the cameras are extrinsically calibrated,

we know the transformations between the camera frames and the world frame. Our algorithm for object pose estimation is to initialize an object pose on the first video frame and then track the object poses in the following frames.

First, using the same object segmentation procedure as described in Section 4.1, we can obtain segmentation masks for each object throughout the sequence. Examples of object segmentation masks are shown in Fig. 5. Second, to estimate the pose of an object in the first video frame, we compute the LoFTR [38] feature matching between the segmented object in the first video frame and all the frames from the video used for the 3D reconstruction of that object (See Fig. 3). The most similar frame from the video for reconstruction is retrieved based on the feature matching, and the 3D rotation of the object \mathbf{R}_0 associated with that frame is used as the initial rotation for the object. The initial translation \mathbf{t}_0 is computed as the center of the segmented point cloud of the object in the world frame, where we utilize aligned depth images from all the cameras to obtain the 3D points of the object in the world frame. The initial object pose will be further refined in the object pose tracking.

SDF-based Object Pose Tracking Once the initial pose of the object $\mathbf{T}_0 = (\mathbf{R}_0, \mathbf{t}_0)$ is computed, we introduce a Signed Distance Field (SDF)-based algorithm to optimize the object poses in the video sequence. We do not adopt BundleSDF for pose tracking in this step since it only supports single-camera input which suffers from severe occlusions during actual manipulation tasks. In contrast, our proposed SDF-based pose tracking leverages the complete point cloud fused from the eight cameras, providing a higher quality pose annotation.

At time step t , our goal is to estimate the object pose \mathbf{T}_t given the previous pose \mathbf{T}_{t-1} , $t = 1, 2, \dots, T$, where T is the total number of frames. We minimize the following loss function

$$\mathbf{T}_t^* = \arg \min_{\mathbf{T}_t} (L_{\text{sdf}}(\mathbf{T}_t) + \lambda_1 L_{\text{smooth}}(\mathbf{T}_t, \mathbf{T}_{t-1})), \quad (1)$$

where λ_1 is a weight to balance the two loss terms. The SDF loss function is defined as

$$L_{\text{sdf}}(\mathbf{T}_t) = \frac{1}{|\mathcal{X}_t|} \sum_{\mathbf{x} \in \mathcal{X}_t} |\text{SDF}(\mathbf{x}, \mathbf{T}_t)|^2, \quad (2)$$

where \mathcal{X}_t denotes a set of 3D points of the object at time step t in the world frame, which is fused from multiple cameras. The function $\text{SDF}(\mathbf{x}, \mathbf{T}_t)$ computes the signed distance of a 3D world point $\mathbf{x} \in \mathbb{R}^3$ transformed into the object frame according to \mathbf{T}_t . Minimizing the SDF loss function finds an object pose such that the transformed 3D points align with the surface of the object model.

The smoothness loss term is defined as

$$L_{\text{smooth}}(\mathbf{T}_t, \mathbf{T}_{t-1}) = \|\mathbf{q}_t - \mathbf{q}_{t-1}\|^2 + \|\mathbf{t}_t - \mathbf{t}_{t-1}\|^2, \quad (3)$$

where \mathbf{q}_t and \mathbf{q}_{t-1} are the quaternions of the 3D rotations, and \mathbf{t}_t and \mathbf{t}_{t-1} denote the 3D translations. The smoothness term prevents large jumps of the

poses during optimization. By solving Eq. (1) for every object and every time step, we obtain the poses of all the objects in the video sequence. These poses provide initializations which will be further refined jointly with the hands, as detailed in Sec. 4.5.

4.3 Hand Shape Reconstruction

Our framework uses the MANO model [?] to represent human hands. This parametric model facilitates the detailed modeling of the human hand mesh using shape and pose parameters: the shape parameters $\beta \in \mathbb{R}^{10}$ capture individual hand identity, reflecting variations across different subjects, while the pose parameters $\theta \in \mathbb{R}^{51}$ describe the dynamic positions and orientations of the hand. We employ the method described in [19], a PyTorch-compatible differentiable implementation of MANO, enabling efficient optimization of hand poses and shapes. Prior to hand pose optimization, we undertake a pre-calibration process for the MANO shape parameters for each subject in our dataset.

We used a three-step process to calibrate the subject’s hand shape. The first step is to conduct an initial pose estimation and collection of 3D points. Starting with a rendered neutral flat MANO hand, participants are instructed to position their right hand to closely match the rendered MANO hand mesh in front of a camera. The 3D points around the hand mesh are collected and dynamically filtered by computing the distance from each 3D point to the mesh surface. This filtering process continues until a sufficient number of 3D points meet a predefined threshold. Then the MANO hand pose is optimized by matching the 3D points to the SDF of the hand model, ensuring the best possible fit to points. Throughout this phase, we fix the shape parameter β at zero, focusing solely on pose optimization. The optimized pose and the set of filtered 3D points are saved for the next step. In the second step, we use the initial pose and points to perform an iterative optimization of both hand shape β and pose θ . We alternate between solving the pose and shape parameters while keeping the other fixed to refine the fit to the collected 3D points. Finally, the optimized hand shape obtained can be further refined by using sequences collected in the dataset. Once the calibration is finished, the hand shape is fixed throughout the following optimization process for hand pose estimation.

4.4 Hand Pose Estimation

In our initial attempts to optimize the hand pose in a video sequence, we endeavored to apply the same loss function utilized in Sec. 4.2 for object pose estimation, anticipating similar success. However, practical experimentation presented significant challenges that required a departure from using the same approach for object pose estimation. A primary issue was the inability to accurately segment the hand using the SAM and XMem methods, which often resulted in the inclusion of arm skin within the segmentation mask. Furthermore, we observed that the higher dimensionality of the MANO hand pose parameter θ , compared

to the 6D pose of objects, led to overfitting when relying solely on a SDF loss, and this overfitting often culminated in the generation of unrealistic hand poses.

To address these challenges, we recognized the need to integrate more robust constraints into our hand pose optimization method. Specifically, we turned to using 2D/3D keypoints of hands as additional constraints. These keypoints, serving as strong priors, significantly anchor the optimization process, thereby ensuring the attainment of more realistic and physically plausible hand poses. At time step t of an input video, our goal is to estimate the MANO hand pose θ_t of a hand. We solve the following optimization problem to estimate hand pose:

$$\theta_t^* = \arg \min_{\theta_t} (L_{\text{keypoint}}(\theta_t) + \lambda_2 L_{\text{reg}}(\theta_t)), \quad (4)$$

where L_{keypoint} is a loss function based on the estimated 3D keypoints of the hand, L_{reg} is a regularization term, and λ_2 is a weight to balance the two terms. The regularization term is simply defined as the squared L2 norm of the pose parameter: $L_{\text{reg}}(\theta_t) = \|\theta_t\|^2$.

3D Keypoint Loss Function We leverage MediaPipe [30] to detect 2D hand landmarks across multiple views. Despite MediaPipe’s ability to identify all 21 hand joints comprehensively, its lack of confidence scoring complicates the identification of occluded or inaccurately estimated joints, potentially leading to inaccuracies in pose optimization.

To overcome these challenges and improve the accuracy of our 3D keypoints, we adopt a RANSAC [?] filtering approach. For a hand joint, let us assume that it is detected by MediaPipe on C_{valid} camera views. Then we can compute a set of candidate 3D keypoints, $\mathcal{X}_i = \{\mathbf{x}_i\}_{i=1}^{N_{\text{valid}}}$, $N_{\text{valid}} = C_{\text{valid}}(C_{\text{valid}} - 1)/2$ by triangulating pairs of valid camera views. A projection loss function is defined for a 3D keypoint:

$$L_{\text{proj}}(\mathbf{x}_i) = \sum_{c \in C_{\text{valid}}} \|H^c(\mathbf{x}_i) - \mathbf{h}_i^c\|^2, \quad (5)$$

where $H^c(\cdot)$ is the projection function for camera c , and \mathbf{h}_i^c represents the detected 2D landmark for the 3D keypoint \mathbf{x}_i in camera c . This loss function measures the discrepancy between each candidate 3D keypoint and its corresponding 2D landmarks on the multi-view images. We minimize it to refine the 3D keypoint position. Finally, the most accurately fitting 3D keypoint for each joint that minimizes the above projection loss function is selected. This critical step ensures the exclusion of views affected by incorrect MediaPipe detections, thereby enhancing the reliability of the derived 3D keypoints. The resulting optimized 3D keypoints, characterized by their precision, are employed as robust priors in subsequent stages of optimization.

For video frames where MediaPipe does not successfully detect hand landmarks across all camera views, we identified that these occurrences constitute a minor fraction of the overall video sequence. Moreover, the temporal proximity of these frames typically exhibits minimal variance in hand pose, suggesting that

linear interpolation between adjacent frames with accurately detected 3D hand joints is a viable strategy for estimating the missing data. Upon addressing these gaps through linear interpolation, we further refine the hand motion trajectory using cubic spline interpolation. This approach ensures smooth transitions not only in the spatial positioning of the hand joints but also maintains continuity in the first and second derivatives of the motion trajectory, corresponding to the velocity and acceleration, respectively. By implementing this technique, we achieve a more natural and cohesive representation of hand motion across the entire sequence, enhancing the realism and fluidity of the observed actions.

Using the estimated 21 3D hand joints $(\mathbf{x}_1, \dots, \mathbf{x}_{21})$, the 3D keypoint loss function is defined as:

$$L_{\text{keypoint}}(\theta_t) = \frac{1}{21} \sum_{i=1}^{21} \|J_i(\theta_t) - \mathbf{x}_i\|^2, \quad (6)$$

where $J_i(\theta_t) \in \mathbb{R}^3$ represents the i th 3D hand joint from the MANO model under pose θ_t . Finally, solving the optimization problem in Eq. (4) will find the MANO hand pose θ_t that fits the estimated 3D keypoints.

4.5 Joint Hand-Object Pose Optimization

Separately solving hand and object poses often results in unrealistic scenarios, such as intersections between the hand mesh and object mesh. To overcome this limitation and improve the accuracy of the pose estimation, we propose a joint pose optimization method. This method optimizes hand and object poses together, addressing mesh intersections and enhancing pose precision.

For a sequence with $N_H \in \{1, 2\}$ hands and N_O objects, at time step t , we jointly refine the object poses $\mathcal{P}_t^O = \{\mathbf{T}_t^o\}_{o=1}^{N_O}$ and hand poses $\mathcal{P}_t^H = \{\theta_t^h\}_{h=1}^{N_H}$. Our idea is to utilize the SDFs of objects and hands to optimize the poses as in our object pose estimation method. The loss function for this joint optimization is defined as

$$L_{\text{joint}}(\mathcal{P}_t^O, \mathcal{P}_t^H) = \frac{1}{N_O} \sum_{o=1}^{N_O} \left(\frac{1}{|\mathcal{X}_t^o|} \sum_{\mathbf{x} \in \mathcal{X}_t^o} |\text{SDF}_o(\mathbf{x}, \mathbf{T}_t^o)|^2 \right) \quad (7)$$

$$+ \frac{1}{N_H} \sum_{h=1}^{N_H} \left(\frac{1}{|\mathcal{X}_t^h|} \sum_{\mathbf{x} \in \mathcal{X}_t^h} |\text{SDF}_h(\mathbf{x}, \theta_t^h)|^2 + \lambda_3 \|\theta_t^h\|^2 \right), \quad (8)$$

where \mathcal{X}_t^o denotes the segmented point cloud for object o at time step t in the world frame, and \mathcal{X}_t^h denotes the segmented point cloud for hand h at time step t in the world frame. SDF_o and SDF_h indicate the signed distance fields of object o and hand h , respectively. λ_3 is a weight to balance the regularization term for the hand pose.

The point clouds of objects can be obtained using the depth images and the segmentation masks of the objects. To obtain point clouds for hands, given the

optimized 3D hand keypoints, we can get the bounding box and 2D keypoints on camera images. Using these 2D keypoints along with the bounding box as input, SAM [22] is employed to generate a high-quality hand mask. A distance threshold of the point-to-mesh distance is applied to further isolate the hand points from the surrounding points using the estimated initial hand pose.

The hand poses and object poses are initialized from the previous stages of the annotation process, and then we solve the joint optimization problem with fewer optimization steps. Our joint pose optimization not only minimizes mesh intersections, but also increases the accuracy and realism of the estimated poses. After estimating the poses of hands and objects in the world frame, we can project the 3D shapes of hands and objects to the camera views and obtain 2D annotations of images as shown in Fig. 5.

4.6 Annotation Quality

In total, we collected 70 videos of 9 participants performing tasks with the 64 objects in our dataset. 3D shapes and poses of hands and objects are generated using our annotation method. To verify the accuracy of our hand-object pose annotations, we randomly selected 800 images from 8 camera views and manually annotated visible hand joints and object keypoints. We calculated the Euclidean distance between our 2D annotations and these manual annotations. The results, shown in Table 2, indicate an annotation error within 5 pixels for both hands and objects, demonstrating high precision. Additionally, an R^2 Score close to 1 confirms the high accuracy of our 2D annotations for hand-object poses. The dataset and the source code of the capture system will be released to the community. Please see the supplementary material for more details about the dataset.

Table 2: Pose verification results (in pixels) for evaluating the accuracy of the provided ground-truth data.

Matrics	Object	Left hand	Right hand
Mean (std)	3.30(\pm 1.70)	4.94(\pm 3.07)	4.56(\pm 2.84)
R^2 score \uparrow	0.999	0.998	0.998

5 Baseline Experiments

After building the dataset, we provide several baseline experimental results to demonstrate the usage of our dataset.

5.1 Hand Pose Estimation

First, our dataset can be used to evaluate hand pose estimation. We provide annotations for 2D positions and 3D positions for the 21 hand joints of human

hands in the dataset. In this experiment, we have evaluated two recent hand pose estimation methods: A2J-Transformer [21] and HaMeR [36], where ground truth bounding boxes of hands are used as input for hand pose estimation. The evaluation results are presented in Table 3. We used the PCK (Percentage of Correct Keypoints) metric for 2D hand pose estimation and the MPJPE (Mean Per Joint Position Error) metric for 3D hand pose estimation. A2J-Transformer extends A2J [46], a depth-based hand pose estimator, to use RGB images as input, and also uses a transformer architecture to encode non-local information. The A2J-Transformer model was trained on the InterHand2.6M dataset [32]. HaMeR [36] uses a large-scale ViT backbone [12] followed by a transformer decoder to regress the parameters of the hand. The HaMeR model was trained on 2.7M images collected from 10 existing hand pose datasets. We can see from Table 3, the performance of HaMeR is significantly better than A2J-Transformer, largely due to using the ViT backbone and large-scale training images. The MPJPE of HaMeR is 29.1mm, which is much larger than the errors reported in other datasets in [36]. This indicates that our dataset poses certain challenges for hand pose estimation, especially occlusions between hands and objects.

Table 3: Evaluation of hand pose estimation. The numbers in parentheses are thresholds for PCK, and unit for MPJPE.

Hand Pose Method	PCK(0.05) \uparrow	PCK(0.1) \uparrow	PCK(0.15) \uparrow	PCK(0.2) \uparrow	MPJPE (mm) \downarrow
A2J-Transformer [21]	4.2	12.0	21.3	31.5	79.6
HaMeR [36]	28.6	66.9	82.8	88.7	29.1

5.2 Novel Object Detection

In this experiment, we consider the problem of novel object detection. In this setup, an object detector is required to detect novel objects that it has not seen during training. We use our dataset to evaluate two baselines for novel object detection: CNOS [34] and GroundingDINO [27]. CNOS [34] is a CAD-based method for novel object detection and segmentation. During testing, 3D CAD models of objects are first rendered to generate image templates. Given an input image, SAM [22] is used to generate region proposals, and these region proposals are compared to the object templates using their DINOv2 cls tokens [35] to classify the region proposals. CNOS uses pre-trained SAM and DINOv2 models. To run CNOS on our dataset, we provide the CAD models of the 64 objects to it. GroundingDINO [27] is a vision-language model for open-set object detection. It can detect objects from input images given text inputs such as category names or referring expressions. We used the concatenation of the object names in our dataset as the text prompt for GroundingDINO.

The evaluation results of the novel object detection are presented in Table 4, where we used the Average Precision (AP) metrics following the MSCOCO metric [26]. In the table, AP is computed for different IoU thresholds and for different object scales. From the table, we can see that both methods do not perform well

on detecting these objects in our dataset for novel object detection. They produce a large number of false alarms. CNOS suffers from mis-matching between region proposals and object templates. For GroundingDINO, using the object names as text prompts is difficult to differentiate the objects in our dataset. The model was confused between different objects. This experiment indicates that better models for novel object detection are worth exploring in future work.

Table 4: Evaluation of novel object detection. The numbers are the mean AP on all 64 objects in our dataset.

Object Detection Method	AP	AP ₅₀	AP ₇₅	AP _S	AP _M	AP _L
CNOS [34]	25.3	27.9	24.8	1.6	27.6	24.9
GroundingDINO [27]	17.0	27.6	21.5	1.4	24.3	7.5

5.3 Novel Object Pose Estimation

Traditional object pose estimation methods such as [11, 45] need to be trained and tested on the same set of objects. Recently, there has been a trend in object pose estimation to develop methods that can be generalized to novel objects that are not seen during training. These methods are trained on a large number of objects, and during testing, given 3D models of novel objects, they can estimate object pose immediately without fine-tuning. In this experiment, we used our dataset as a test bed and evaluated two recent methods for novel object pose estimation: MegaPose [24] and FoundationPose [44]. Ground truth 2D bounding boxes of objects are used as input for the pose estimation methods. The evaluation results are presented in Table 5, where we used the AUC of ADD and ADD-S metrics that are widely used for object pose estimation [11, 45]. The state-of-art method FoundationPose [44] outperforms MegaPose [24] by a considerable margin, likely due to the power of its transformer-based architecture with large scale synthetic training. This aligns with the results as reported in [44]. Fig. 6 shows an example of pose estimation from these two methods.

Table 5: Evaluation of object pose estimation for novel objects. The numbers are the AUC percentage of the ADD and ADD-S metrics on all 64 objects in our dataset.

Object Pose Method	ADD (%)	ADD-S (%)
MegaPose [24]	62.3	81.6
FoundationPose [44]	81.6	93.9

6 Limitations

Our annotation framework has two limitations related to the methods used in the annotation process. First, we saw that BuddleSDF [43] cannot reconstruct

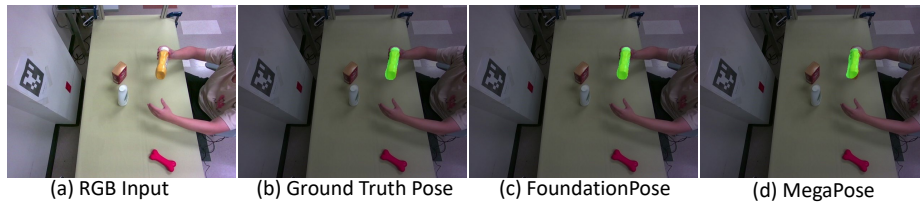


Fig. 6: Visualization of object pose estimation results

certain types of objects very well, such as some textureless objects and metal objects. Therefore, we were unable to include these objects in our dataset. Second, MediaPipe [30] has failures in detecting human hand joints. Since our hand pose estimation is based on the hand joints detected by MediaPipe, once it cannot detect that hand joints, we cannot obtain the hand poses. We excluded some videos in which MediaPipe failed to detect human hands.

7 Conclusion

We introduced a new capture system and a new dataset for hand-object intersection. Our system uses multiple RGB-D cameras and a HoloLens headset for data collection. It captures videos from both third-person views and first-person views. A semi-automatic annotation method is proposed to obtain 3D shapes and poses of hands and objects in the collected videos. The method leverages pre-trained large-scale vision models for 3D object reconstruction, object segmentation, object pose estimation, and hand joint detection, where no domain-specific training is required during the annotation process. In addition, an SDF-based optimization algorithm is introduced to refine the hand pose and object pose. Consequently, using the capture system and the annotation method, we contribute the HO-Cap dataset that contains human actions of using objects to perform various tasks. The dataset can be used to study hand-object interaction, as well as serving as a human demonstration dataset for embodied AI and robotics manipulation research.

Acknowledgement. This work was supported in part by the DARPA Perceptually-enabled Task Guidance (PTG) Program under contract number HR00112220005 and the Sony Research Award Program.

References

1. Microsoft hololens. <https://www.microsoft.com/en-us/hololens> 2, 5
2. Microsoft kinect. <https://azure.microsoft.com/en-us/services/kinect-dk> 5
3. Vicalib. <https://github.com/arp/vicalib> 5
4. Brahmabhatt, S., Tang, C., Twigg, C.D., Kemp, C.C., Hays, J.: Contactpose: A dataset of grasps with object contact and hand pose. In: Computer Vision–ECCV 2020: 16th European Conference, Glasgow, UK, August 23–28, 2020, Proceedings, Part XIII 16. pp. 361–378. Springer (2020) 2, 4

5. Calli, B., Walsman, A., Singh, A., Srinivasa, S., Abbeel, P., Dollar, A.M.: Benchmarking in manipulation research: The ycb object and model set and benchmarking protocols. arXiv preprint arXiv:1502.03143 (2015) [6](#)
6. Castro, P., Kim, T.K.: Crt-6d: Fast 6d object pose estimation with cascaded refinement transformers. In: Proceedings of the IEEE/CVF Winter Conference on Applications of Computer Vision. pp. 5746–5755 (2023) [1](#)
7. Chao, Y.W., Yang, W., Xiang, Y., Molchanov, P., Handa, A., Tremblay, J., Narang, Y.S., Van Wyk, K., Iqbal, U., Birchfield, S., et al.: Dexycb: A benchmark for capturing hand grasping of objects. In: Proceedings of the IEEE/CVF Conference on Computer Vision and Pattern Recognition. pp. 9044–9053 (2021) [1](#), [2](#), [4](#)
8. Chen, Z., Chen, S., Schmid, C., Laptev, I.: gsdf: Geometry-driven signed distance functions for 3d hand-object reconstruction. In: Proceedings of the IEEE/CVF Conference on Computer Vision and Pattern Recognition. pp. 12890–12900 (2023) [1](#)
9. Cheng, H.K., Schwing, A.G.: Xmem: Long-term video object segmentation with an atkinson-shiffrin memory model. In: European Conference on Computer Vision. pp. 640–658. Springer (2022) [2](#), [6](#)
10. Darkhalil, A., Shan, D., Zhu, B., Ma, J., Kar, A., Higgins, R., Fidler, S., Fouhey, D., Damen, D.: Epic-kitchens visor benchmark: Video segmentations and object relations. *Advances in Neural Information Processing Systems* **35**, 13745–13758 (2022) [1](#)
11. Deng, X., Mousavian, A., Xiang, Y., Xia, F., Bretl, T., Fox, D.: Poserbpf: A rao-blackwellized particle filter for 6-d object pose tracking. *IEEE Transactions on Robotics* **37**(5), 1328–1342 (2021) [14](#)
12. Dosovitskiy, A., Beyer, L., Kolesnikov, A., Weissenborn, D., Zhai, X., Unterthiner, T., Dehghani, M., Minderer, M., Heigold, G., Gelly, S., et al.: An image is worth 16x16 words: Transformers for image recognition at scale. arXiv preprint arXiv:2010.11929 (2020) [13](#)
13. Fan, Z., Taheri, O., Tzionas, D., Kocabas, M., Kaufmann, M., Black, M.J., Hilliges, O.: Arctic: A dataset for dexterous bimanual hand-object manipulation. In: Proceedings of the IEEE/CVF Conference on Computer Vision and Pattern Recognition. pp. 12943–12954 (2023) [1](#), [2](#), [4](#)
14. Garcia-Hernando, G., Yuan, S., Baek, S., Kim, T.K.: First-person hand action benchmark with rgb-d videos and 3d hand pose annotations. In: Proceedings of the IEEE conference on computer vision and pattern recognition. pp. 409–419 (2018) [4](#)
15. Ge, L., Cai, Y., Weng, J., Yuan, J.: Hand pointnet: 3d hand pose estimation using point sets. In: Proceedings of the IEEE conference on computer vision and pattern recognition. pp. 8417–8426 (2018) [1](#)
16. Gong, J., Foo, L.G., Fan, Z., Ke, Q., Rahmani, H., Liu, J.: Diffpose: Toward more reliable 3d pose estimation. In: Proceedings of the IEEE/CVF Conference on Computer Vision and Pattern Recognition. pp. 13041–13051 (2023) [1](#)
17. Guo, A., Wen, B., Yuan, J., Tremblay, J., Tyree, S., Smith, J., Birchfield, S.: Handal: A dataset of real-world manipulable object categories with pose annotations, affordances, and reconstructions. In: 2023 IEEE/RSJ International Conference on Intelligent Robots and Systems (IROS). pp. 11428–11435. IEEE (2023) [4](#)
18. Hampali, S., Rad, M., Oberweger, M., Lepetit, V.: Honnotate: A method for 3d annotation of hand and object poses. In: Proceedings of the IEEE/CVF conference on computer vision and pattern recognition. pp. 3196–3206 (2020) [2](#), [4](#)

19. Hasson, Y., Varol, G., Tzionas, D., Kalevatykh, I., Black, M.J., Laptev, I., Schmid, C.: Learning joint reconstruction of hands and manipulated objects. In: Proceedings of the IEEE/CVF conference on computer vision and pattern recognition. pp. 11807–11816 (2019) [4](#), [9](#)
20. Jian, J., Liu, X., Li, M., Hu, R., Liu, J.: Affordpose: A large-scale dataset of hand-object interactions with affordance-driven hand pose. In: Proceedings of the IEEE/CVF International Conference on Computer Vision. pp. 14713–14724 (2023) [1](#), [4](#)
21. Jiang, C., Xiao, Y., Wu, C., Zhang, M., Zheng, J., Cao, Z., Zhou, J.T.: A2j-transformer: Anchor-to-joint transformer network for 3d interacting hand pose estimation from a single rgb image. In: Proceedings of the IEEE/CVF Conference on Computer Vision and Pattern Recognition. pp. 8846–8855 (2023) [13](#), [20](#), [21](#)
22. Kirillov, A., Mintun, E., Ravi, N., Mao, H., Rolland, C., Gustafson, L., Xiao, T., Whitehead, S., Berg, A.C., Lo, W.Y., et al.: Segment anything. arXiv preprint arXiv:2304.02643 (2023) [2](#), [4](#), [6](#), [12](#), [13](#)
23. Kwon, T., Tekin, B., Stühmer, J., Bogo, F., Pollefeys, M.: H2o: Two hands manipulating objects for first person interaction recognition. In: Proceedings of the IEEE/CVF International Conference on Computer Vision. pp. 10138–10148 (2021) [1](#), [2](#), [4](#)
24. Labbé, Y., Manuelli, L., Mousavian, A., Tyree, S., Birchfield, S., Tremblay, J., Carpentier, J., Aubry, M., Fox, D., Sivic, J.: Megapose: 6d pose estimation of novel objects via render & compare. arXiv preprint arXiv:2212.06870 (2022) [14](#), [23](#), [24](#)
25. Lee, T., Tremblay, J., Blukis, V., Wen, B., Lee, B.U., Shin, I., Birchfield, S., Kweon, I.S., Yoon, K.J.: Tta-cope: Test-time adaptation for category-level object pose estimation. In: Proceedings of the IEEE/CVF Conference on Computer Vision and Pattern Recognition. pp. 21285–21295 (2023) [1](#)
26. Lin, T.Y., Maire, M., Belongie, S., Hays, J., Perona, P., Ramanan, D., Dollár, P., Zitnick, C.L.: Microsoft coco: Common objects in context. In: Computer Vision—ECCV 2014: 13th European Conference, Zurich, Switzerland, September 6–12, 2014, Proceedings, Part V 13. pp. 740–755. Springer (2014) [13](#)
27. Liu, S., Zeng, Z., Ren, T., Li, F., Zhang, H., Yang, J., Li, C., Yang, J., Su, H., Zhu, J., et al.: Grounding dino: Marrying dino with grounded pre-training for open-set object detection. arXiv preprint arXiv:2303.05499 (2023) [13](#), [14](#), [20](#)
28. Liu, Y., Liu, Y., Jiang, C., Lyu, K., Wan, W., Shen, H., Liang, B., Fu, Z., Wang, H., Yi, L.: Hoi4d: A 4d egocentric dataset for category-level human-object interaction. In: Proceedings of the IEEE/CVF Conference on Computer Vision and Pattern Recognition. pp. 21013–21022 (2022) [1](#), [2](#), [4](#)
29. Lorensen, W.E., Cline, H.E.: Marching cubes: A high resolution 3d surface construction algorithm. In: Seminal graphics: pioneering efforts that shaped the field, pp. 347–353 (1998) [7](#)
30. Liguori, C., Tang, J., Nash, H., McClanahan, C., Uboweja, E., Hays, M., Zhang, F., Chang, C.L., Yong, M., Lee, J., Chang, W.T., Hua, W., Georg, M., Grundmann, M.: Mediapipe: A framework for perceiving and processing reality (2019), https://mixedreality.cs.cornell.edu/s/NewTitle_May1_MediaPipe_CVPR_CV4ARVR_Workshop_2019.pdf [2](#), [10](#), [15](#)
31. Mittal, A., Zisserman, A., Torr, P.H.: Hand detection using multiple proposals. In: BMVC. vol. 2, p. 5. Citeseer (2011) [1](#)

32. Moon, G., Yu, S.I., Wen, H., Shiratori, T., Lee, K.M.: Interhand2.6m: A dataset and baseline for 3d interacting hand pose estimation from a single rgb image. In: Computer Vision–ECCV 2020: 16th European Conference, Glasgow, UK, August 23–28, 2020, Proceedings, Part XX 16. pp. 548–564. Springer (2020) [13](#)
33. Mueller, F., Davis, M., Bernard, F., Sotnychenko, O., Verschoor, M., Otaduy, M.A., Casas, D., Theobalt, C.: Real-time pose and shape reconstruction of two interacting hands with a single depth camera. *ACM Transactions on Graphics (ToG)* **38**(4), 1–13 (2019) [1](#)
34. Nguyen, V.N., Groueix, T., Ponimatkin, G., Lepetit, V., Hodan, T.: Cnos: A strong baseline for cad-based novel object segmentation. In: Proceedings of the IEEE/CVF International Conference on Computer Vision. pp. 2134–2140 (2023) [13](#), [14](#), [20](#)
35. Oquab, M., Darcet, T., Moutakanni, T., Vo, H., Szafraniec, M., Khalidov, V., Fernandez, P., Haziza, D., Massa, F., El-Nouby, A., et al.: Dinov2: Learning robust visual features without supervision. *arXiv preprint arXiv:2304.07193* (2023) [13](#)
36. Pavlakos, G., Shan, D., Radosavovic, I., Kanazawa, A., Fouhey, D., Malik, J.: Reconstructing hands in 3d with transformers. *arXiv preprint arXiv:2312.05251* (2023) [1](#), [13](#), [20](#), [21](#)
37. Shan, D., Geng, J., Shu, M., Fouhey, D.F.: Understanding human hands in contact at internet scale. In: Proceedings of the IEEE/CVF conference on computer vision and pattern recognition. pp. 9869–9878 (2020) [1](#)
38. Sun, J., Shen, Z., Wang, Y., Bao, H., Zhou, X.: Loftr: Detector-free local feature matching with transformers. In: Proceedings of the IEEE/CVF conference on computer vision and pattern recognition. pp. 8922–8931 (2021) [6](#), [8](#)
39. Swamy, A., Leroy, V., Weinzaepfel, P., Baradel, F., Galaoui, S., Brégier, R., Armando, M., Franco, J.S., Rogez, G.: Showme: Benchmarking object-agnostic hand-object 3d reconstruction. In: Proceedings of the IEEE/CVF International Conference on Computer Vision. pp. 1935–1944 (2023) [4](#), [6](#)
40. Taheri, O., Ghorbani, N., Black, M.J., Tzionas, D.: Grab: A dataset of whole-body human grasping of objects. In: Computer Vision–ECCV 2020: 16th European Conference, Glasgow, UK, August 23–28, 2020, Proceedings, Part IV 16. pp. 581–600. Springer (2020) [4](#)
41. Tu, Z., Huang, Z., Chen, Y., Kang, D., Bao, L., Yang, B., Yuan, J.: Consistent 3d hand reconstruction in video via self-supervised learning. *IEEE Transactions on Pattern Analysis and Machine Intelligence* (2023) [1](#)
42. Wen, B., Bekris, K.: Bundletrack: 6d pose tracking for novel objects without instance or category-level 3d models. In: 2021 IEEE/RSJ International Conference on Intelligent Robots and Systems (IROS). pp. 8067–8074. IEEE (2021) [2](#)
43. Wen, B., Tremblay, J., Blukis, V., Tyree, S., Muller, T., Evans, A., Fox, D., Kautz, J., Birchfield, S.: Bundlesdf: Neural 6-dof tracking and 3d reconstruction of unknown objects. *CVPR* (2023) [1](#), [2](#), [6](#), [14](#)
44. Wen, B., Yang, W., Kautz, J., Birchfield, S.: Foundationpose: Unified 6d pose estimation and tracking of novel objects. *arXiv preprint arXiv:2312.08344* (2023) [1](#), [14](#), [23](#), [24](#)
45. Xiang, Y., Schmidt, T., Narayanan, V., Fox, D.: Posecnn: A convolutional neural network for 6d object pose estimation in cluttered scenes. *arXiv preprint arXiv:1711.00199* (2017) [1](#), [14](#)
46. Xiong, F., Zhang, B., Xiao, Y., Cao, Z., Yu, T., Zhou, J.T., Yuan, J.: A2j: Anchor-to-joint regression network for 3d articulated pose estimation from a single depth image. In: Proceedings of the IEEE/CVF International Conference on Computer Vision. pp. 793–802 (2019) [13](#)

47. Yang, L., Li, K., Zhan, X., Wu, F., Xu, A., Liu, L., Lu, C.: Oakink: A large-scale knowledge repository for understanding hand-object interaction. In: Proceedings of the IEEE/CVF Conference on Computer Vision and Pattern Recognition. pp. 20953–20962 (2022) [1](#), [2](#), [4](#)
48. Yingze Bao, S., Chandraker, M., Lin, Y., Savarese, S.: Dense object reconstruction with semantic priors. In: Proceedings of the IEEE conference on computer vision and pattern recognition. pp. 1264–1271 (2013) [1](#)
49. Zhang, F., Bazarevsky, V., Vakunov, A., Tkachenka, A., Sung, G., Chang, C.L., Grundmann, M.: Mediapipe hands: On-device real-time hand tracking. arXiv preprint arXiv:2006.10214 (2020) [1](#)

Appendix

A Experimental Details

We have benchmarked three tasks using our dataset: hand pose estimation, novel object detection, and novel object pose estimation. To enhance the efficiency of the evaluation, all methods are evaluated using sampled keyframes in our dataset.

For 6D object pose estimation, given the significant occlusion observed at the two lowest camera angles and the high proportion of hands in the egocentric perspective, we selected 12,781 frames from the remaining six viewpoints for evaluation. These chosen frames encompass diverse poses of objects. We use the ground truth bounding boxes as input for the pose estimation methods.

For hand pose estimation, the evaluation frames were decimated to a frequency of 10 frames per second (FPS) across the eight RealSense cameras, yielding a total of 207,208 frames. This subsampled dataset is deemed adequately comprehensive to capture the variety of hand poses.

For 2D object detection, a random sampling strategy was employed to select 10,632 frames for analysis from the RealSense camera feeds.

B Qualitative: 3D Hand Pose Estimation

Fig. 7 shows qualitative results of 3D hand pose estimation using HaMeR [36] and A2J-Transformer [21] methods. As shown in the figure, the results include both 2D hand joints and 3D hand joints. HaMeR demonstrates superior accuracy in hand pose estimation compared to A2J-Transformer. Due to the limitations of the A2J-Transformer training process, it lacks consideration for the interaction between the hand and surrounding objects. The results show that as the interaction area between the hand and the object increases or when the hand is occluded by the object, the performance of A2J-Transformer deteriorates. Conversely, HaMeR exhibits a robust adaptability to these challenging conditions by training a ViT model with large-scale training images.

C Qualitative: Novel Object Detection

Fig. 8 shows qualitative results of 2D novel object detections with GroundingDINO [27] and CNOS [34]. We used the combined object product names as prompt captions for GroundingDINO. For CNOS, we create feature templates for each object by rendering the textured 3D model from different views. Both methods produce a significant number of false alarms when testing our data. Since there are only four objects for each scene, the qualitative results in Fig. 8 only show the top-four detected bounding boxes with the highest detection scores.

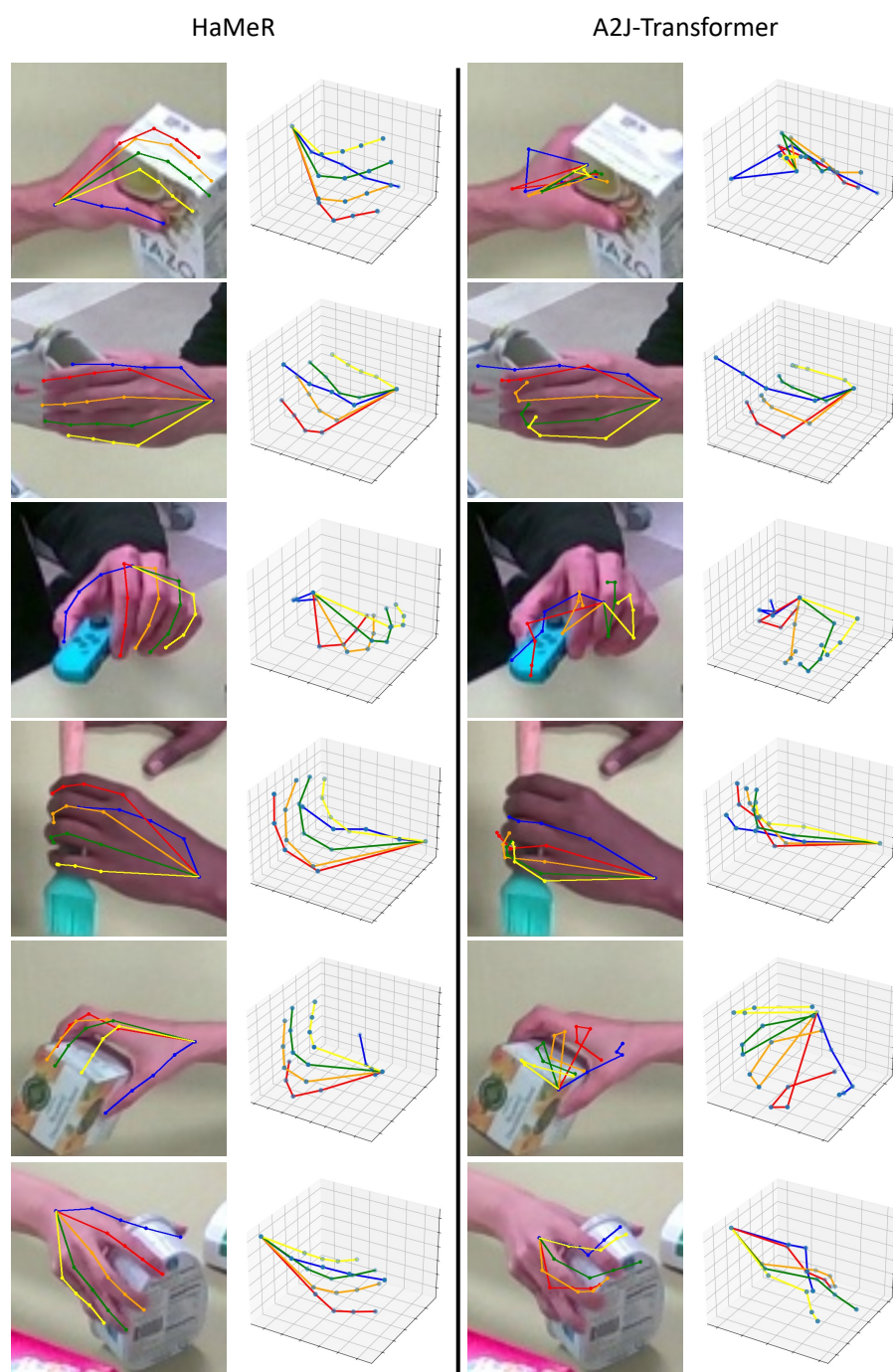


Fig. 7: Qualitative results of the predicted 3D hand pose using HaMeR [36] (left two columns) and A2J-Transformer [21] (right two columns).



Fig. 8: Qualitative results for novel object detection

D Qualitative: 6D Object Pose Estimation

Fig. 9 shows qualitative results of 6D object pose estimation. We render the object models given the estimated poses and overlay them on top of a darkened input image. We can see that FoundationPose [44] generates more accurate 6D pose predictions than MegaPose [24] on novel objects.

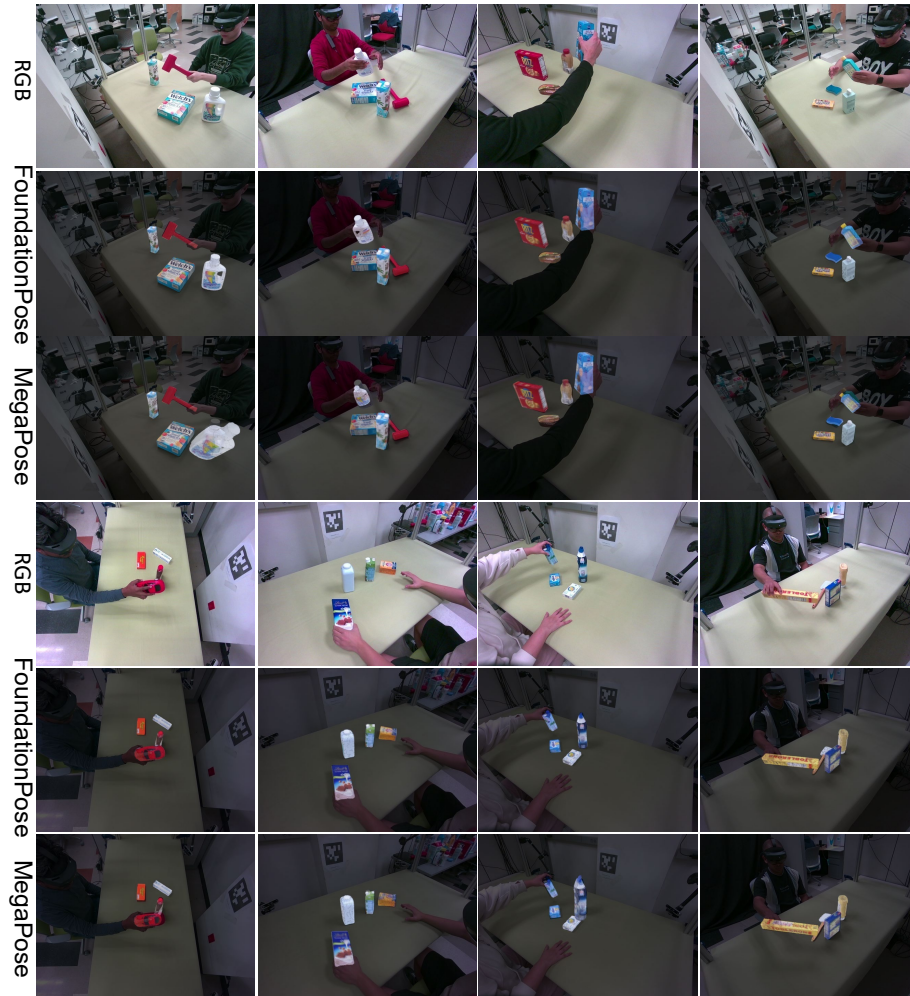


Fig. 9: Qualitative results of 6D object pose estimation. (Top to down: Input RGB frame, FoundationPose [44], MegaPose [24])

E Quantitative: 6D Object Pose Estimation

For 6D object pose estimation, we include more detailed results for the evaluation metrics—namely, Average Distance (ADD) and Symmetric Average Distance (ADD-S)—on a per-object basis in Table 6. The relationships of objects and their IDs can be found in Fig. 10. We observe that FoundationPose [44] significantly surpasses MegaPose [24] in handling novel objects, demonstrating a substantial improvement in accuracy.

Object ID	FoundtionPose [44]		MegaPose [24]		Object ID	FoundtionPose [44]		MegaPose [24]	
	ADD	ADD-S	ADD	ADD-S		ADD	ADD-S	ADD	ADD-S
G01_1	95.92	93.50	93.55	88.83	G11_1	93.85	81.17	81.21	61.33
G01_2	96.00	93.00	88.16	79.76	G11_2	93.86	80.98	81.14	61.04
G01_3	95.74	89.28	81.72	69.68	G11_3	93.91	81.21	81.28	60.89
G01_4	95.20	83.67	81.99	66.30	G11_4	93.28	80.78	80.54	60.29
G02_1	95.42	79.74	82.62	63.10	G15_1	93.30	80.85	80.51	60.23
G02_2	95.55	82.23	84.30	66.20	G15_2	93.31	80.92	80.53	60.22
G02_3	95.70	84.08	85.39	67.49	G15_3	93.33	80.95	80.54	60.24
G02_4	95.61	85.10	84.94	67.21	G15_4	93.31	80.97	80.46	60.23
G04_1	95.56	85.27	84.15	66.17	G16_1	93.38	81.23	80.54	60.61
G04_2	95.61	85.69	84.10	65.67	G16_2	93.35	80.80	80.57	60.39
G04_3	95.29	85.56	84.03	65.85	G16_3	93.42	81.06	80.40	60.34
G04_4	95.31	85.86	84.43	66.75	G16_4	93.25	80.98	80.30	60.40
G05_1	94.94	85.34	84.12	66.12	G18_1	93.26	80.55	80.31	60.00
G05_2	95.10	86.37	83.81	65.68	G18_2	93.17	80.35	80.30	59.94
G05_3	95.11	85.88	83.96	65.72	G18_3	93.18	80.37	80.39	60.12
G05_4	95.01	81.57	84.23	63.42	G18_4	93.17	80.43	80.50	60.36
G06_1	94.95	82.87	84.42	64.53	G19_1	93.11	80.15	80.52	60.39
G06_2	95.11	84.22	83.81	63.50	G19_2	93.11	80.26	79.97	60.20
G06_3	95.23	81.01	84.14	61.89	G19_3	93.19	79.02	79.92	59.34
G06_4	93.18	79.49	80.84	59.70	G19_4	93.07	78.69	79.99	59.29
G07_1	93.20	79.76	80.45	59.71	G20_1	93.11	78.83	80.06	58.86
G07_2	93.29	80.09	80.54	59.97	G20_2	93.15	79.00	80.17	59.00
G07_3	93.29	80.32	80.64	60.36	G20_3	93.18	79.13	80.31	59.26
G07_4	93.30	80.54	80.53	60.59	G20_4	93.07	78.84	80.08	58.71
G09_1	93.38	80.76	81.01	61.46	G21_1	93.20	79.28	80.46	59.01
G09_2	93.41	81.38	81.49	62.79	G21_2	93.07	79.27	80.57	59.30
G09_3	93.52	80.27	81.60	61.83	G21_3	92.38	78.71	79.08	58.20
G09_4	93.70	81.14	81.79	62.08	G21_4	92.16	78.47	78.09	57.47
G10_1	93.77	81.42	81.93	62.33	G22_1	92.20	78.53	78.21	57.64
G10_2	93.82	81.27	82.00	62.14	G22_2	92.20	77.75	78.11	57.07
G10_3	93.79	81.45	82.04	62.39	G22_3	92.23	77.90	78.14	57.09
G10_4	93.79	80.91	81.58	61.62	G22_4	92.26	78.02	78.03	57.05

Table 6: 6D object pose estimation results of representative approaches in ADD and ADD-S.



Fig. 10: Objects with their IDs in our dataset.